submitted to *Geophys. J. Int.*

Volcanic deformation and flank instability due to magmatic sources and frictional rheology: the case of Mount Etna

S. Cianetti[1], C. Giunchi[1] and E. Casarotti[2]

[1]*Istituto Nazionale di Geofisica e Vulcanologia, Via della Faggiola 32, 56126 Pisa, Italy*

[2]*Istituto Nazionale di Geofisica e Vulcanologia, Via di Vigna Murata 605, 00143 Roma, Italy*

3 August 2012

SUMMARY

The overall picture of Mount Etna deformation emerging since a couple of decades of geodetic surveys shows effects of magma accumulation, characterized by inflation/deflation cycle, accompanied by a sliding instability of the southeast flank, whose manifestation is an increase in the horizontal deformation away from the volcano summit. This is a very interesting case to test whether advanced models, taking into account topography, internal structure and frictional rheology, may contribute to a better understanding of the complex interplay among mechanical response, magmatic activity and gravitational load occurring in a volcanic system. Using finite element numerical models we make predictions of surface displacements associated with a simple expansion source and with a dike like vertical discontinuity. A new methodology is developed to initalize the lithostatic stress field according to the material and geometrical complexities of the models considered. Our results show that, while an amplification of the horizontal displacement can be easily obtained up to a maximum distance of 10 km from the source, we have not been able to find any configuration to extend further this signal. For the case of Mount Etna this suggests that the large horizontal displacements observed in the east flank along the coast cannot be directly related to magma accumulation below the volcano's summit.

Key words: volcanic deformation – Mount Etna – frictional rheology – flank instability.

1 INTRODUCTION

Volcanic deformation is the surface expression of the internal dynamics of an inherently complex system resulting from the interaction of magma with the surrounding rocks. Additionally, active volcanoes are often affected by some kind of long or short term instability influenced by the development and growth of the edifice in presence of gravity field and/or other tectonic forces (McGuire 1996). Not only surface deformation records the simultaneous interplay between the magmatic activity and the edifice instability, but it may also be strongly affected by vertical and lateral variations of the mechanical properties of the volcano, ambient stress state, strain rate and temperature conditions. Our purpose is to understand to which extent the surface deformation caused by a simple magmatic source, such as a pressurized spheric cavity, is altered by the above mentioned factors. Among the large number of active volcanoes experiencing edifice instability, Mount Etna, whose structure and activity are well studied, represents an interesting test case to evaluate the role of these heterogeneities. Zooming out from the single deformation episodes, we aspire to study the link between the general features of the observed ground deformation and some configurations of the internal structure that are likely to characterize Mount Etna. The model is contrived accounting for both topography and the top of the sedimentary basement, together with a synthetic reconstruction of the internal layering constrained by geology and seismic tomography (Fig. 1). The rheological parameters of the Etnean lithotypes are settled by laboratory experiments conducted in the framework of the FLANK INGV-DPC project. We study a series of 2D models to understand the role of gravity, internal layering, rheology, and sliding planes considering as active source either an isotropic spherical cavity (0.5 km radius) located at 5 km b.s.l. or a vertical dike.

The outline of the paper is the following. We summarize in section 2 the deformation observed at Mount Etna and discuss its interpretation according to some of the past modelling attempts. In section 3 we describe all the a-priori information utilized in the numerical models, together with the constraints on material properties. In particular, we address how to perform a self-consistent initialization of the lithostatic stress field (section 3.4). In section 4 we show the effects on the pre-

dicted deformation patterns due to different sources and different configurations of the rheological layering. Finally, we discuss about the implications for Mount Etna flank instability (section 5).

2 MOUNT ETNA DEFORMATION

Ground deformation at Mount Etna has been extensively monitored by local geodetic networks and satellite observations for about 25 years or more. Recently published papers by Solaro et al. (2010) and Bonforte et al. (2011) have analysed and interpreted the deformation history between 1994 and 2008. These studies have taken advantage of satellite interferograms processed by different techniques and their results suggest at least three main processes with clear signatures in the observed deformation. The first is an overall inflation/deflation of the volcanic edifice, whose source, located a few km northwest of the summit craters, exhibits a radial pattern of horizontal motions. The second process is related to dike emplacement along pre-existing well known structures aligned north-south or northeast-southwest. The third is a marked instability of the east flank characterized by a very complex pattern dominated by an increase of the horizontal velocities from the summit craters to the coast. While the first two mechanisms can be considered directly related to magmatic activity (magma accumulation at depth or near the surface), the flank instability has the peculiarity to persist during slow recharge phases with no paroxysmal activity (such as from 1993 to 1997) or to manifestly accelerate after summit eruptions (such as 2001 and 2002-2003 events). This suggests that the east flank instability is somehow linked to the internal structure and the overall mechanical response of Mount Etna.

Despite the increasing availability of geodetic data, robust inference of the location and properties of the magmatic sources is still very difficult as evidenced by the huge number of modelling papers attaining results only in partial agreement. The problem is twofold: on one side surface observations show the superposition of multiple simultaneous processes; on the other side the forward models proposed are often an inaccurate approximation of reality. One of the most explicative example concerns the definition of the 1993-1997 source parameters. There is a general agreement among researchers to consider this time period, due to the absence of summit activity, as one of the most suitable to study the inflation source. Nevertheless, as showed by Bonforte et al.

(2008, Table 4) who summarized previous results based on the interpretation of GPS data, there is a scatter about source depth determinations as large as 6 km or more (roughly between 2 and 8 km b.s.l.). Researchers dealing with this dataset came soon up to the conclusion that model predictions remain far from fitting the observed data, even increasing the complexity of forward models, including for example, different source shapes, topography and internal material heterogeneities (Bonaccorso et al. 2005), or temperature dependent viscoelastic rheology (Del Negro et al. 2009).

The need to discriminate between the contribution of magma accumulation and the sliding in the east flank led to different approaches (Lundgren & Rosen 2003; Lundgren et al. 2004; Bonaccorso et al. 2005; Bonforte & Puglisi 2006; Currenti et al. 2007; Palano et al. 2008; Trasatti et al. 2008; Aloisi et al. 2011b; Bonforte et al. 2011). Some authors just neglected GPS benchmarks affected by seaward drift, trying to clean up the inflation/deflation signal to attempt a better determination of the inflation source (Aloisi et al. 2011a). An effort to consider the full GPS/SAR observations has been done by Trasatti et al. (2009) adding to the inflation source, a rigid translation of a prescribed block representing the east flank. Other authors tried to explain the whole geodetic signal taking into account supplementary deformation sources such as southeast dipping sub-horizontal faults (Bonforte & Puglisi 2006; Bonforte et al. 2008) or southeast and west dipping fault planes (Lundgren & Rosen 2003; Lundgren et al. 2004). The goal for these models is the search of the best fitting source parameters relative to a restricted time period. Once sources have been identified they have to be framed in the complex volcanic system of Mount Etna. However, it is not always possible to reconcile these results with evidence coming from seismology, stratigraphy, geochemistry and structural geology. Just as an example, the southeast dipping sub-horizontal fault, that should mimic a sliding surface accommodating the seaward sliding of the volcano, poorly reconcile with the absence of any seismological fingerprints (Gambino et al. 2004). The fact that earthquake distributions do not image a buried discontinuity below the east flank suggests that the observed motion may be accommodated by anelastic deformation occurring inside a layer of non-coherent clays trapped between the volcanic edifice and the Pleistocenic flysch (Tibaldi & Groppelli 2002). Nevertheless, this idea is not fully supported by geological evidence since these

clays outcrop only in a few sites and their extension as a continuous layer below the east side of Mount Etna is purely speculative (Neri & Rossi 2002).

The main criticism to the concept of a widespread east flank instability is that this would cause a clear evidence at its front, where the observation of compressional structures such as anticlines is expected. However, even the latest off-shore geophysical investigations (Chiocci et al. (2011) and Argnani et al. (2011)) provide results that cannot be directly considered as clear signatures of the seaward sliding of the east flank, again showing the absence of compressional anticlines (Pareschi et al. 2006). While Chiocci et al. (2011) focus more on the role of a large scale off-shore gravitational instability that triggers the movements observed in the sub-aerial flank, conclusions by Argnani et al. (2011) are much more articulated on the different times in which the observed structures have been active. However, both Chiocci et al. (2011) and Argnani et al. (2011) agree that the morphological complexity of the Ionian continental margin and regional tectonics have to be taken into account to explain the evolution of Mount Etna.

As a consequence, none of these studies provide a satisfying insight into the dynamics behind the mechanism of the flank seaward drift. There is still an open debate about many interesting themes: $i)$ the depth of the sliding surface and whether it is affecting a thin (Bonforte & Puglisi 2006; Bonforte et al. 2008) or thick (Neri et al. 2005; Ruch et al. 2010) portion of the east flank; $ii)$ what are the geometry and the surface boundaries of the volume involved (Solaro et al. 2010; Bonforte et al. 2011); $iii)$ which is the relationship between the sliding and the magmatic eruptive cycle (inflation - eruption) (Acocella & Neri 2003; Battaglia et al. 2011; Bonaccorso et al. 2011); $iv)$ what is the role played by gravity (Aloisi et al. 2011b) compared to stratigraphical (Tibaldi & Groppelli 2002), seismological (De Gori et al. 2005), geophysical/geochemical (Siniscalchi et al. 2010), seismic reflection (Chiocci et al. 2011) and petrological (Corsaro & Pompilio 2004) evidence.

Our contribution to this debate is to study a general model not specifically targeted to explain a single event, but aimed to understand how the introduction of structural and/or rheological complexities affect the predicted deformation pattern. To check whether predictions may resemble the observed signals, it may be useful, however, to make a semi-quantitative comparison with data

taken from the real deformation patterns. To this purpose we refer to the continuous GPS (CGPS) data collected between May 2008 and December 2010 by Etn@net (Aloisi et al. 2011b; Palano et al. 2010), which show the persistence of some general features of the Mount Etna ground deformation already summarized by Solaro et al. (2010) and Bonforte et al. (2008) for the period 1994-2008. Aloisi et al. (2011b) suggest to classify the volcano activity phases based on the areal dilatation of benchmarks placed in proximity to the summit craters compared to others placed at intermediate altitude. Among the phases identified by Aloisi et al. (2011b) we select (Fig. 2) two periods (June 2009-May 2009 and May 2010-December 2010, respectively) to extrapolate the horizontal and vertical deformation rates and hopefully show some characteristic trends for Mount Etna. For these phases we have projected the ground deformation along the cross section AA′ of Fig. 1 for those GPS stations whose distance from AA′ is less than 4 km (benchmarks falling within the two black solid lines). These data are also fitted by a cubic polynomial to better show the deformation pattern. The two time periods are characterized by inflation accompanied by a marked seaward sliding of the east flank, with an increase of observed rates from the volcano summit toward the Ionian Sea. While in the period June 2009-May 2009 (Fig. 2a-b) a large seaward sliding in the east flank is associated to subsidence of GPS benchmarks at a distance greater than 10 km from the summit, in the period May 2010-December 2010 (Fig. 2c-d) the overall inflation signal is reduced in amplitude but all the GPS data show moderate uplift along the cross section.

3 MODELLING

3.1 Model setup

The complex volcano-tectonic environment of Mount Etna is characterized by several major structural lineaments (red lines in Fig. 1a). Some of these structures are well imaged by surface signatures: the Pernicana fault delimiting the northern border; the northeast and south rifts defining the northeastern and western boundary of the sliding sector; the Mascalucia-Tremestieri and the Santa Venerina faults and the Timpe Fault Systems internal to the **east** flank. Others have been identified thanks to the analysis of InSAR data (Solaro et al. 2010) but do not correspond to well known tectonic structures. These lineaments certainly play a role in the east flank dynamics. However,

apart from surface signatures, it is very difficult to constrain their depth extent using, for example, seismic tomography imaging or seismic moment release data. For this reason we limit our attention to a 2D plane strain cross section assumed to be representative of the central part of the **east** flank and depicted in Fig 1b.

Internal geometry is defined on the basis of stratigraphical constraints (Borgia et al. 1992; Tibaldi & Groppelli 2002; Bousquet & Lanzafame 2004). The section shown in Fig 1b is the result of a cooperation within the numerical modelling task of the INGV-DPC project "FLANK", whose scientific coordinators promoted the compilation of shared database of relevant features of Mount Etna (Acocella & Puglisi 2010; Norini & Acocella 2011). The following lithotypes (Fig. 1b) have been selected as first order representation of the Mount Etna structure: Volcanites (the upper cover due to past and recent effusive activity), Flysch (heterogeneous sedimentary layer resulting from the continental collision process of Hyblean foreland), Carbonates (Mesozoic-Cenozoic sequence of Hyblean foreland). In addition to this basic structure we take into account two further elements: a dike complex volume (DC hereinafter) underneath summit craters imaged by seismic tomography (Chiarabba et al. 2004; Patanè et al. 2006), and Clays, an intra-pleistocenic clay layer which can likely favour the decoupling between Volcanites and Flysch.

The topography of the interface between Flysch and Volcanites is obtained from Neri & Rossi (2002) (see contour lines in Fig. 1a). Its surface is characterized by a cone-shaped geometry reaching 1300 a.s.l. further northwest with respect to the summit craters. This surface is potentially important because it may accommodate the seaward sliding of the volcanic cover. The geological maps of Mount Etna (e.g. Monaco et al. 2010) show that some infra-pleistocenic clay outcrops are present in correspondence of this layer in the southeastern sector of Mount Etna (Neri & Rossi 2002).

These Pleistocenic clays, due to their cohesion-less properties, may accommodate a large internal deformation allowing the sliding of the volcanic sediments above. Unfortunately, these outcrops are few and spread in a large area with spot-like distribution: the presence of an extended and continuous sediments layer below the whole eastern flank is purely speculative. Nonetheless, since neither tomography nor geology investigations definitely support either a sliding interface or

a low-cohesion clays layer in this paper we account for both the hypotheses. Below this interface, up to 4 km depth, the Pleistocenic Flysch of the Hyblean foreland is described as a melange of sandstones and clays characterized by extremely different rheological parameters. While the arenaceous component shows a weak behaviour, the marly and clayeous part are very strong. How the two end-members combine and if one prevails over the other is not known also due to the large extension of the sedimentary sequence. It is difficult to reconcile these differences in a single material due to the possible prevalence of one of the sedimentary component over the other as well as the feasible role of the geometry of the melange. The choice will be inevitably subjective and questionable but necessary. Deeper, at almost 4 km depth, the mixed sandstone-clay layer meets the carbonatic platform. Although the rheology of the carbonatic sequence is less disputable, large uncertainties concern the geometry of this interface. There is a general agreement that this boundary deepens eastward probably due to the role of the normal faults pertaining to the Malta escarpment. This complex interface has been here simplified with a step like, seaward deepening, geometry (Norini & Acocella 2011).

Stratigraphic constraints are integrated with indirect observations, such as that derived from seismic tomography, to provide an exhaustive picture not only of regional but also of the local scale processes. Indeed interpretations of v_p and v_p/v_s anomalies have significant implications on the fluid content and rock alteration that may be important factors of the east flank dynamics. The scientific community agrees that a relevant structural element of Mount Etna is the large volume of high v_p anomaly below the summit craters imaged by seismic tomography (Patanè et al. 2003; Chiarabba et al. 2004; Patanè et al. 2006). This "cold" and basically aseismic anomaly has deep roots and crosses the Pleistocenic flysch up to a depth of about 1 km b.s.l. (Patanè et al. 2006). The uppermost part of this high v_p volume can be interpreted as the dike complex DC formed by repeated intrusion episodes, as suggested by Tibaldi & Groppelli (2002). It is quite clear that this first order inhomogeneous structure inside Mount Etna may play a significant role both during magma ascent episodes (Puglisi et al. 2008) as well as in disrupting the symmetry of the deformation induced by the inferred pressurized bodies (Bonaccorso et al. 2005; Currenti et al. 2010).

3.2 Mesh and boundary conditions

The 2D plane strain cross section shown in Fig. 1b and described in Sec. 3.1 extends 170 $\times$ 30 km and has been discretized into 108528 4-node isoparametric elements. The grid resolution ranges between 45 m in proximity of maximum expected deformation area (e.g. the volcanites and the pressurized source) and 500 m at the boundaries. A pressurized source located 5 km b.s.l. is sketched as a sphere of radius $r = 500$ m. The very simple geometry of the source is determined by our purpose to verify what kind of heterogeneity is able to produce an asymmetric deformation pattern compatible with observations. To the source is applied a $\Delta P_{\text{source}} = P_m - P_l = 35$ MPa, where P_m and P_l are the magmatic and lithostatic pressures, respectively. This value is considered as a threshold value above which we suppose that the magma rises upward through a complex distribution of conduits. We have drastically simplified the real geometry of these upraising paths by a vertical single dike connecting the magmatic source to the surface. This predefined discontinuity is loaded by a pressure reduced to $\Delta P_{\text{dike}} = 5$ MPa. The values of both ΔP_{source} and ΔP_{dike} ensure that predicted surface displacements are of the same order of those observed by geodetic networks. The vertical dike surface is characterized by a stick-slip friction law with a dynamic effective friction coefficient $\mu' = 0.2$, while the static friction is 1.05 times larger. Analogous contact properties are applied to the sub-horizontal discontinuity (when included) extending at the Volcanites/Flysch interface that should mimic the sliding surface accommodating the flank instability. The choice of the value of $\mu' = 0.2$ is compatible with the results obtained by Dieterich (1988) analysing a model for rift-flank interaction. We have verified that higher values of μ' prevent any relative motion along the sub-horizontal sliding plane due to the predominance of the lithostatic load.

The model initial condition is a pre-assigned lithostatic stress, whose computation, in presence of topography and material heterogeneities, is not trivial because it requires to apply the gravity load preserving the original undeformed geometry of the mesh. The details of the computations are exhaustively described in Sec. 3.4. The other boundary conditions are: fixed vertical displacement of the base; semi-infinite boundary elements at the lateral margins; atmospheric pressure at the free surface; gravity load as body force.

3.3 Material properties

The mechanical properties of the lithotypes representative of the internal structure of Mount Etna have been constrained by laboratory investigations. Samples of each lithotype have been collected by S. Vinciguerra and their physical properties measured at the HP-HT Laboratory at INGV Roma (Heap et al. 2011; Mollo et al. 2011). Many assumptions are needed in order to use these experimental measurements in the numerical modelling: *i)* four lithotypes are a limited subset of the larger variability observed; *ii)* measurements conducted on a limited number of small (few centimetres) samples are supposed to be representative of units as large as tens of kilometres, neglecting local scale inhomogeneities; *iii)* the experiments are conducted in the framework of laboratory conditions which are different from natural conditions; *iv)* last but not least laboratory experiments do not provide a unique value for the investigated parameter, suggesting instead a range of values for each parameter. Among the parameters provided by laboratory experiments we are interested in: Young's Modulus, Poisson's ratio, density, and Uniaxial Compression Strength (UCS). These rheological parameters allow us to describe the elastic-frictional behaviour of the rocks at low pressure and temperature using the Drucker-Prager model. The Drucker-Prager parameters were computed from Mohr-Coulomb equivalent values using the relationship shown in Cianetti et al. (2008, eq. 2, 3), while a discussion about the significance of employing Drucker-Prager to describe brittle rock deformation can be found in Albert et al. (2000, pag. 406). Since the experiments were conducted in uniaxial configuration, we fixed the internal friction angles to values measured in rocks of the same type (Peng & Zhang 2007, Table 3.1). All the mechanical parameters used in the numerical models are provided in Table 1. Carbonates and DC materials are considered just for their elastic properties and not for the frictional behaviour. We also neglect any effects due to the temperature distribution or thermally activated creep, being deformation mechanisms usually taking place at greater depths.

3.4 Initializing lithostatic stress

One of the issues we are concerned about is the role of gravity in the east flank sliding, therefore, it is imperative to include the gravity load into the models. Initialization of lithostatic stress is

not a trivial problem if we want to take into account topography, lateral variations of material properties such as the density, or non-linear rheology that depends on the stress tensor and on the deformation history. In this paper we develop an original iterative procedure to retrieve the lithostatic initial stress consistent with the actual shape of the volcano, the assumed rheology and material properties. The lithostatic stress computed with the iterative procedure is then used as the initial reference stress for further computations. This ensure us to obtain an undeformed geometry under a stress condition of lithostatic equilibrium. It may be argued that this is not appropriate for Mount Etna, a volcano settled in an area geodynamically active due to Calabrian Arc subduction. However, in this paper we are not dealing with tectonic stresses, but we try to understand if gravitational instability may represent the main cause of the eastern flank collapse. So we believe that considering the edifice, built up by repeated eruptions, in isostatic equilibrium is a good approximation to test the effects of magma inflation and dike emplacement as well as the role of frictional rheology probably controlling the layer of unconsolidated clay that is supposed to be located between volcanites and sedimentary rocks.

The idea (sketched in Fig. 3) is to apply a gravity load to the model with no preassigned stress conditions and compute the deformation and stress fields. The volcano deforms under its own weight (the whole domain is compressed by some hundred meters). The stress field due to gravity load is used as the initial stress in a new model with the original undeformed geometry and the same loading conditions. In the second iteration the computed deformation is one order of magnitude smaller with respect to the first step. A new stress field is retrieved and used as the initial stress of the original undeformed model (third step). The resulting vertical compression further reduces. The iterative procedure is repeated until the initial stress approximates the isostatic equilibrium. The convergence to the lithostatic equilibrium may require a small or large number of iterations according to the assumed material properties: in the case of purely elastic material the reference stress tensor is easily found in few steps (virtually one for flat topography and depth dependent density anomaly); if we deal with a plastic rheology (material deforms at constant stress above a threshold value) the iterative procedure should be repeated until computed displacements are small compared to the deformation we want to investigate. It is not *a priori* possible to guess

if the convergence to the isostatic equilibrium can be achieved. Indeed, plastic material may be characterized by a stress threshold so small to be considered cohesion-less implying that it is always deforming never being able to relax the internal stress below the intrinsic threshold.

How important is it to initialize the stress field in the proper material configuration? What is the effect of a change of the materials rheology at the end of the iteration procedure? Fig. 4 shows the total equivalent plastic strain for three different stress initialization assumptions. In the computations the deformation source is the pressurized cavity. Plasticity is confined in a thin layer located between the volcanic edifice and the sedimentary basement. In Fig. 4a the stress is not initialized. When the source is pressurized, the stress accumulated in the plastic layer induces a deformation with a maximum total equivalent plastic strain of 0.016 s^{-1}. If the stress is initialized assuming that the layer is elastic during the iteration procedure and that the rheology changes to plastic when the source is pressurized (Fig. 4b), then the maximum total equivalent plastic strain reduces to 0.012 s^{-1}, slightly smaller than the previous one. But if we initialize the stress considering the proper rheology for the plastic layer from the beginning (Fig. 4c) then we observe that a large amount of the stress is dissipated in the initialization process and the maximum total equivalent plastic strain reduces to 0.002 s^{-1}, one order of magnitude smaller than the latter model. This means that, applying the same forcing to the three models, the predicted displacements are different. In particular the latter predicts a displacement much smaller with respect to the others. These computational examples clearly enlighten the importance to a stress initialization compatible with rheological parameters of the model. For this reason, we have computed a consistent initial stress for each model presented throughout this paper.

3.5 Outline of the models

As reference and benchmark with analytical solutions and previously published papers, we first consider an elastic homogeneous model with topography (Fig. 5a). According to the stratigraphic reconstruction described in Sec. 3.1 we move to the model depicted in Fig. 5b that includes the main stratigraphic units (Volcanites, Flysch and Carbonates) and the DC. The model is further developed including the infra-pleistocenic clays layer between the Volcanites and the Flysch (Fig. 5c)

according to the hypothesis that the unconsolidated clays may deform either for gravitational forcing or be driven by source inflation and/or dike emplacements. Moreover, we test the surface displacement sensitivity to variations of DC extension (Fig. 5d). The lively debate about the mechanism accommodating the eastward sliding of Mount Etna's flank will be addressed in section 4.4 where a sliding surface instead of a compliant Clay layer is considered.

4 RESULTS

Models results will be provided as normalized displacements because we are not interested in fitting a single dataset but we want to understand how deformation in the east flank is accumulated in response to various system configurations. Nevertheless, all the results, shown as normalized displacements, are characterized by a surface deformation in agreement with typical values observed (models predict about 10 cm of surface uplift for the expansion source and about 1 m of horizontal displacement for the dike source, respectively).

4.1 Shape of the magmatic reservoir

Fig. 6a shows the horizontal and vertical displacements normalized by the maximum vertical displacements for spherical and ellipsoidal magmatic sources in a poissonian homogeneous elastic half-space (Mogi 1958). For spherical sources the ratio $U_x^{\max}/U_z^{\max} = 0.4$ is a well defined value not influenced by source depth and dimension. Displacement is, of course, symmetric.

Let us start here evaluating the amount of asymmetry derived from a non-spherical magmatic source. Fig. 6b-d shows $U_x/U_z^{\max}$ and $U_z/U_z^{\max}$ for an oblate ($a = b = 5c$), prolate ($a = 5b = 5c$) and oblique ($a = 2b = 5c$ and dip angle = 45°) ellipsoidal cavity (Davis 1986), respectively, where a, b, c are the semimajor axes of the ellipsoid. Both for oblate and prolate ellipsoids the predicted displacements are symmetric but vanish in a shorter distance with respect to the Mogi model. In the case of the oblique ellipsoid (Fig. 6d) the symmetry of the displacement is broken, especially for the horizontal component. Finally, we want to remark that for all these analytical models $U_z^{\max}$ is always much larger than $U_x^{\max}$ while this is not true for signals observed at Mount Etna.

4.2 Isotropic source in a complex medium

How are the predicted displacements affected by an isotropic source embedded in a medium characterized by some sort of heterogeneities? Let us consider Mount Etna topography as the first cause of dissimilarity (Fig. 5, model REF). Although the general trend of the curves shown in Fig. 7a looks like the homogeneous flat one, being still very symmetric, there are some major differences: *i)* $U_z/U_z^{\max}$ now has two maxima separated by a local minimum located just above the source center; *ii)* $U_x^{\max}/U_z^{\max} \neq 0.4$; *iii)* $U_x/U_z^{\max}$ decays to zero slower than the flat case; *iv)* $U_x/U_z^{\max}$ shows an inflection point at the cavity center. At this point we introduce the internal structure of the volcano inferred from structural and tomographic studies (Fig. 5, model LAY). Now the predicted displacements (Fig. 7b) are strongly asymmetric. The $U_z^{\max}$ is shifted southeastward. The $U_x^{\max}$ is closer to the source center and decays with distance very slowly. However, also in this case we are not able to reproduce the observed horizontal displacements that suggest a rigid block sliding toward the southeast. To enhance the development of a flank instability and sliding we hypothesize that a uniform layer of unconsolidated clays exists between Volcanites and Sandstones (model CLAY in Fig. 5). We assume that this layer deforms accordingly to a Drucker-Prager rheology. Fig. 7c shows the corresponding normalized displacement curves. They are very similar to those in Fig. 7b but the $U_x/U_z^{\max}$ has a maximum smaller than the previous even though it maintains a higher value over larger distance from the source (more congruous to a rigid sliding). We also test the sensitivity of the model increasing the dimensions of DC above the inflation source (model DC-CLAY in Fig. 5). The predicted displacement (Fig. 7d) is strongly asymmetric. A local minimum develops above the reservoir, while $U_x^{\max}/U_z^{\max}$ increases with respect to model CLAY.

4.3 Dike opening and frictional rheology

In the following we introduce a new deformation source represented by a vertical dike placed below the summit craters. Using CLAY as reference model we consider two cases characterized by different dike extensions: a shallow one, crossing only the volcanic cover (SD-CLAY) and a second one reaching the magmatic expansion reservoir (DD-CLAY). Fig. 8 shows the predicted normal-

ized horizontal and vertical displacements for models SD-CLAY and DD-CLAY together with the normalized observed data (Aloisi et al. 2011b, phases 3 and 4) when: only the spheric source is active (Fig. 8a, b); only the dike is pressurized (Fig. 8c, d). In the first case the dike is considered as a passive pre-existing discontinuity able to release some of the deviatoric stress provided by the isotropic expanding source located below. Keep in mind that the purpose here is not to find best fitting parameter for this dataset but just to catch the main features of the observed deformation. The comparison with the dataset from Fig. 2 (normalized and replotted in Fig. 8) is performed just to check the discrepancy between model predictions and observed surface deformation.

The comparison between model CLAY (Fig. 7c) and models SD-CLAY (Fig. 8a) and DD-CLAY (Fig. 8b) shows that $U_z^{\max}$ is always larger than $U_x^{\max}$ and the ratio $U_x^{\max}/U_z^{\max}$ changes from $\sim$0.5 to $\sim$0.7. A well developed U_z local minimum is now predicted above the magmatic sources. U_z is positive up to $\sim$ 15 km and continues slightly negative after that. The displacement curves are continuous suggesting that no shear movement occurs along the dike, and neither opening reaches the surface. However, the deformation patterns are different from what are predicted in model CLAY suggesting that the dikes should play a role even though not that relevant. Indeed, the differences between surface displacements for models SD-CLAY and DD-CLAY are really small indicating that the isotropic source has an overall similar behaviour in both models resulting in the opening at depth between 2.3 and 1.1 km a.s.l. of the dikes (1 cm and 5 cm maximum opening, respectively). Since 1.1 km a.s.l. corresponds to the top of the clay layer, we speculate that the stress release induced by the deep magmatic source promotes frictional deformation in the clay layer causing an unclamping of the dike segment above it. The slightly larger displacement computed for model DD-CLAY is due to the small vertical propagation (100 m length) of the deepest part of the dike just above the magma chamber. Comparing the normalized ground deformation to normalized data collected during time interval June 2009 – May 2010 shows that the trends are different, the greatest discrepancy being observed for U_z: while geodetic displacement is characterized by diffuse subsidence starting less than 5 km from the summit craters, the model prediction signal is positive or weakly negative (15 km away of the deformation center). Focusing on the May 2010 – December 2010 time interval a partial agreement between data and predictions

may be speculated either for horizontal and vertical components. Despite that the predicted eastward displacements are large compared to those obtained by uniform models, the retrieved trend is always characterized by a maximum located approximately 8-9 km from the craters and a gentle slow decay toward the Ionian Sea. The geodetic dataset, on the other hand, places the maximum amplitude at almost 15-20 km from the craters. None of the proposed models is able to reproduce this feature suggesting that the frictional deformation in the Clays layer is not efficient enough to allow the overriding volcanic cover to move eastward as a rigid block. We have also tested lower values of cohesion for the Clays layer but, in these cases the volcanic cover is continuously drifting eastward due to the effect of gravity, and the isostatic equilibrium cannot be attained (see Section 3.4 for details). The predicted displacement indeed amounts to hundreds if not thousands of meters, an unrealistic value for Mount Etna.

Fig. 8c, d show the normalized horizontal and vertical displacements predicted by the active dike opening. The first thing we note is that $U_x^{\max}$ is now larger than $U_z^{\max}$. Both U_x and U_z are discontinuous at the surface, with opening prevailing over shear movement. $U_x^{\max}$ is located about 2.5 km east of the summit and decays more rapidly with distance with respect to what is predicted when the magmatic source at depth is active (Fig. 8a, b). U_z, also characterized by two relative maxima in proximity to the summit, reverses its sign at between 5 to 10 km, and remains close to zero at greater distances . Both horizontal and vertical displacements are almost symmetric with respect to the deformation center meaning that, even the active dike source is not able to cause any significant frictional deformation in the compliant Clays layer, despite being very close (model SD-CLAY) or even in direct contact with it (model DD-CLAY).

4.4 Sliding plane

Let us now explore how ground deformation changes when the soft Pleistocenic clay layer is replaced by a sub-horizontal sliding plane running between the volcanic cover (Volcanites) and the sedimentary Flysch considering the models SD-PLAY and DD-PLAY in Fig. 9. Comparing deformation produced by the pressurized isotropic source for models SD-PLAY (Fig. 9a) and SD-CLAY (Fig. 8a) we note that the effect of the sliding plane is to enhance the asymmetry either in

horizontal and vertical directions. This suggests that the surface of discontinuity located between the Volcanites and the Flysch transfers deformation more efficiently with respect to the Clays layer. Here, the dike opens (10 cm maximum opening) and slides at depth between 2.9 km and 1.1 km a.s.l.. Moreover, the first 400 m of the sub-horizontal plane closer to the dike slides eastward favouring the asymmetric deformation pattern. $U_x^{\max}/U_z^{\max}$ is now 0.9 while $U_x^{\min}/U_z^{\max}$ is as low as -0.5. $U_x^{\max}$ is always achieved $\sim$7 km away from the summit and then gently reduces in amplitude. The most important feature retrieved by this model is that U_x reverses its sign $\sim$2 km west of the sumit while the U_z local minimum persists over the deformation source. As for CLAY models $U_z^{\max}$ is larger than $U_x^{\max}$ and $U_z \simeq 0$ for distances $\gtrsim \pm 15$ km. What happens if the dike is not confined to the volcanic cover but extends deeper to the magmatic source as for DD-PLAY model? Now the differences in Fig. 9b are noticeable because the dike slides all along its length resulting in a discontinuous vertical displacement at surface. Dike opening is confined between 2.1 km and 1.1 km a.s.l. and between 3.6 km and 4.2 km b.s.l.. The sub-horizontal discontinuity does not slide. The resulting ground horizontal deformation is characterized by two local maxima, the smallest above the dike and the largest further east of the summit but not far enough to fit the observed data. U_x changes its sign almost 4 km west of the summit. In this model $U_z^{\min}$ is negative just above the dike in agreement with observations. Left and right of the minimum the model predicts two very asymmetric relative maxima. Then U_z approaches to zero never assuming the large negative values recorded on the east flank.

We consider now the vertical dike as active source (Fig. 9c,d) using the same boundary conditions as the models SD-CLAY and DD-PLAY (Fig. 8c,d). Some of the observations we have already done for model SD-CLAY can be repeated also for model SD-PLAY (Fig. 9c): $U_x^{\max}$ is larger than $U_z^{\max}$; ground deformation is more symmetric; U_z decays to zero very quickly; U_z is weakly negative around 4 km east of the summit but not enough to approximate observations. In the case of the deeper dike (Fig. 9d, model DD-PLAY) the surface displacements show a significant opening and shearing along the dike resulting in a strong asymmetric deformation pattern. Predicted vertical and horizontal movements are almost completely confined to the east flank. The comparison with the normalized data relative to June 2009 – May 2010 and May 2010 –

December 2010 (Aloisi et al. 2011b, phase 3 and 4, respectively), shows that, despite a slight improvement with respect to model series CLAY, none of the proposed computations is able to model the negative vertical displacement recorded at the eastern GPS benchmarks where also the maximum horizontal deformation is observed. Moreover, we are not able to fit, at the same time, both horizontal and vertical deformations and the west and east sectors of the volcano as well. For example model DD-PLAY in Fig. 9b shows that west of the summit the horizontal displacement well approximates May 2010 – December 2010 data while vertical deformation agrees with June 2009 – May 2010 observations. In the east flank predicted vertical displacements are characterized by a strong uplift not evidenced by data, while the maximum of horizontal displacements is still located at about 5 km from the summit.

To give a contribution to the open debate about the role of a shallow or deep sliding plane accommodating eastward sliding of the east flank of Mount Etna we have taken into account a model with a sliding surface located at the base of the Clays layer of Fig. 5 (1.5 km b.s.l.) and emerging $\sim$ 40 km east of the summit craters. For this model the results slightly differ (less than 5%) from those plotted in Fig. 9b, d. However, in order to get the same amount of surface deformation a reduction of the effective friction coefficient along the sliding plane from $\mu' = 0.2$ to 0.1 is needed. It might be surprising that a deepening of the sliding plane of 2 km or more provides a comparable deformation to the shallow plane delimited by the Volcanites/Flysch layers. We recall that sliding occurs along the predefined discontinuity if the ratio between shear and normal stresses overcomes the effective static friction coefficient. The deeper plane is closer to the source and certainly it is subject to an higher shear stress but also to an higher lithostatic load, while the shallower plane, being more distant from the source, undergoes a lower shear stress from the source, but an equally decreased lithostatic load. The results are similar because the higher distance from the source of the shallower plane is compensated by the higher lithostatic load of the deeper plane resulting in similar shear/normal stress ratio. As a consequence, in both cases eastward sliding takes place only along a segment of about 5-8 km from the source so that the surface deformation is quite similar. We emphasize that the lithostatic load is a critical factor to prevent the sliding along a sub-horizontal interface, and this is also confirmed by the fact that even

the halving of μ' for the deeper plane does not allow the sliding to propagate for more than 8 km from the source.

4.5 Volcanic cycle

The usual approach in volcano deformation modelling is to account for a forward or inverse model aimed to the interpretation of a specific data set collected in a well defined time-interval. In nature, however, every deformation episode is just an event in the volcano evolution. If this approximation is justified in the case of a purely elastic rheology where the effects of every source are additive, this is not the case when dealing with frictional plastic rheology where the final deformation depends on the sequence in which loads are applied. Our purpose here is to evaluate how model predictions may change if we neglect the fact that every single deformation episode is just one part of a complex deformation history. One simple way is to setup a model where an inflation and deflation cycle is repeated numerous times. The recent activity of Mount Etna may suggest a cycle consisting of 3 years inflation followed by a rapid 3 months deflation. In Fig. 10 this inflation/deflation cycle is repeated 5 times. Both DD-CLAY and DD-PLAY models have been forced applying a $\Delta P_{\mathrm{source}}$ to the spherical source reaching 35 MPa after 3 years and decreasing to zero in 3 months (purple dashed lines in Fig. 10). It is interesting to note that either the frictional layer in DD-CLAY or the sliding plane in DD-PLAY affect the displacement of the surface point considered only in the first couple of cycles. Afterwards, displacements follow the time evolution of the source suggesting that the system is turned to a conservative one and basically only the elastic properties of the materials are significant. The U_x and U_z displacements in Fig. 10a are only moderately affected by the small frictional deformation developed in model DD-CLAY during the first cycle. This indicates that the applied $\Delta P_{\mathrm{source}}$ is not large enough to induce a significant frictional deformation able to influence the displacement recorded at the top surface. In the following cycles an essentially elastic behaviour with full recover of the deformation after the load removal is observed. Conversely, model DD-PLAY U_x and U_z (Fig. 10b) are strongly influenced by the movements along the sliding plane. After two cycles the horizontal and vertical displacements stop showing the sawtooth behaviour of the first cycle and sensibly reduce in amplitude. In

the first inflation the contact surface between Volcanites and Flysch layers slides with the typical stick-slip behaviour to release the shear stress accumulated due to the magmatic source. From the third cycle on, again an elastic, conservative response is observed. The oscillations due to sliding during the inflation phase of the first cycle lead to a final position very close to that of the following cycles ($\sim$ 9 cm for U_z and $\sim$ 6 cm for U_x). This is not true for the final position of the deflation phase which is $\sim$ -2 cm both for U_x and U_z, while in the other cycles the values are $\sim$ 4 cm and $\sim$ 2 cm for U_x and U_z, respectively. This probably can be explained by considering that in the deflation phase the recovery of the elastic part of the deformation is also inhibited by the gravity load, preventing any back sliding on the sub-horizontal discontinuity. The results of this simplified model of recharge/discharge of a volcanic system are based on the hypothesis that the source reaches the same $\Delta P_{\mathrm{source}}$. This certainly may be a very strong and conservative approximation. Nonetheless our results show that the repeated action of the stress due to magma accumulation may induce the smearing of the signatures due to non-linearities such as frictional/plastic deformation or sliding planes, turning the system into an apparent conservative state dominated by elastic response. Of course, in case of strong increase of overpressure at the source, the system may again will be forced to release the stress reactivating the frictional deformation or sliding. For the specific case of Mount Etna, these results suggest that it is unlikely that the flank instability is maintained active by the action of a magmatic source because this would require a continuous rising of the deviatoric stress.

5 IMPLICATIONS FOR MOUNT ETNA FLANK INSTABILITY

The flank instability is a very complex and multi-factor peculiarity of the east side of Mount Etna which results from the complex interplay between forces due to magma intrusions, gravity and tectonics acting in a heterogeneous environment such as a volcanic edifice. In the last few years each of these mechanisms has been reclaimed and proposed as the most important factor according to the data or model analysed. For example, both Solaro et al. (2010) and Bonforte et al. (2011), analysing surface deformation from InSAR observations using similar processing algorithms, conclude that gravitational instability and block segmentation are the key factors to de-

scribe the observed data. On the other hand, both Norini & Acocella (2011) and Bonaccorso et al. (2011), by means of analogue or numerical modelling, suggest that a combination of magmatic activity, asymmetric boundary conditions with feedback on flank instability have to be considered the first order processes. Other papers instead focus on the leading role of dike type intrusions in the presence of elastic heterogeneities (Aloisi et al. 2011b) or consider the tectonic environment within which Mount Etna is embedded as the responsible to drive the entire evolution of the system (Chiocci et al. 2011). From this simple and incomplete review of the latest published papers, we can notice how, despite the increasing amount of high quality data produced by the geophysics and geodetic monitoring networks deployed, the possibility to discriminate between causal effects of the various processes involved seems still very far from being addressed.

In this paper we have been looking for a combination of structural features, rheological properties and active sources being able to focus a significant amount of horizontal deformation away from the volcano summit, which is the most important manifestation of flank instability. Despite the limitations of the 2 dimensional modelling which restricts our considerations to the AA' cross section, our computations suggest that at mid high altitudes and up to a distance of about 10 km, there are some factors very efficient in providing an asymmetric horizontal displacement distribution between east and west flanks, as demonstrated by the results in Figs. 7, 8 and 9. Among these factors the most important are: frictional rheology, elastic heterogeneities associated to the presence of the asymmetric DC volume, the vertical dike discontinuity below the summit craters and the sub-horizontal sliding plane. This study suggests that a careful inference of the source parameters based on deformation data should be aware of effects of these elements. At lower elevations and larger distances from the volcano summit, approaching the coast, the flank instability cannot be directly related to magma accumulation. Indeed, none of the models we investigated has been able to transfer a significant amount of horizontal deformation up the coast line where large deformations have been recorded, also associated with a negative vertical displacement, never predicted by our computations. Our findings support the hypothesis that the sliding at low elevations could be related to local, shallow-depth, structures. This view is as well supported by DInSAR deformation in the last 15 years and the seismic activity. DInSAR data show clear evidence of

a deformation field partitioned into blocks with coherent internal behaviour (Solaro et al. 2010; Bonforte et al. 2011). On the other hand, seismic studies such as Alparone et al. (2011); Patanè et al. (2005) suggest that the earthquake hypocenter distribution reveals an evident connection only with the major structures delimiting the flank, such as the Pernicana fault: within the flank, seismic activity is quite scattered especially for its depth distribution and its relationship with the recognized surface structures is rather puzzling and unclear. This missing link supports the hypothesis that the flank dynamics at low elevations can be conditioned by the mechanical properties of the uppermost layers and does not involve deep structures.

6 CONCLUSIONS

The goal of this paper has been to study the surface deformation caused by simple sources embedded in a layered domain with frictional rheology resembling a 2D section of Mount Etna across the east flank. Taking full advantage of the *a priori* information about the internal structure we have studied the predicted deformation checking for the effects of compliant layers or sliding planes.

Symmetry of surface deformation induced by isotropic sources and ratio between horizontal and vertical components can be disrupted in the case of a layered structure and/or lateral heterogeneities. We have shown that anisotropic sources in a homogeneous, isotropic and poissonian half-space provide a lesser degree of asymmetry when compared to isotropic sources embedded in a layered and laterally heterogeneous domain. For the specific case of Mount Etna, the DC volume underneath summit craters significantly contributes to increase the deformation in the east sector.

The frictional rheology is endorsed because it provides a more realistic stress distribution, while purely elastic models can easily predict deviatoric stress levels non sustainable by crustal rocks. On the other hand, it requires a consistent initialization of the stress field. We have shown that, according to different assumptions about the initial stress distribution, different results can be obtained due to a total or partial relaxation of the differential stress due to the gravity load. This result suggests that initial stress assumptions can severely influence the assessment of the physical mechanisms that may lead to flank instability.

For the two episodes of Mount Etna deformation considered we find that our modelling is

effective to enhance deformation in the east flank up to 10 km from the source. However, the high rates of horizontal displacements observed in the sites at larger distances and lower altitudes require a further mechanism in addition to the isotropic source, dyke opening and sliding planes included in the modelling.

When a longer time span is considered, which encompasses several inflation-deflation cycles, the overall frictional response may be reduced due to the deviatoric stress relaxation by frictional/plastic deformation as long as there is no significant increase in magma overpressure among the subsequent cycles. In other words the hysteresis loop is substantially reduced after the first cycle and the system quickly tends toward an elastic behaviour where the deformation is almost totally recovered. This model, predicting variations in the mechanical response of the volcanic system as a function of the loading history, suggests another important element that may impact the interpretation of volcanic deformation.

ACKNOWLEDGMENTS

We thank the GJI AE J. Wassermann, P. Lundgren and an anonymous referee for their constructive comments. S. Vinciguerra and the HPHT Laboratory team at INGV, M Aloisi and M. Bisson provided laboratory experiments data, GPS data and Mount Etna topography. We thank F. Mazzarini for fruitful discussions and enthusiastic encouragement. The research activity was funded by the INGV-DPC project V4 FLANK" whose coordinators V. Acocella and G. Puglisi are acknowledged for support.

REFERENCES

Acocella, V. & Neri, M., 2003. What makes flank eruptions? The 2001 Etna eruption and its possible triggering mechanisms, *Bulletin of Volcanology*, **65**(7), 517–529.

Acocella, V. & Puglisi, G., 2010. Hazard Mitigation of Unstable Volcanic Edifices, *EOS, Trans., AGU*, **91**(40).

Albert, R., Phillips, R., Dombard, A., & Brown, C., 2000. A test of the validity of yield strength envelopes with an elastoviscoplastic finite element model, *Geophysical Journal International*, **140**(2), 399–409.

Aloisi, M., Mattia, M., Ferlito, C., Palano, M., Bruno, V., & Cannavò, F., 2011a. Imaging the multi-level magma reservoir at Mt. Etna volcano (Italy), *Geophysical Research Letters*, **38**, L16306.

Aloisi, M., Mattia, M., Monaco, C., & Pulvirenti, F., 2011b. Magma, faults, and gravitational loading at Mount Etna: The 2002-2003 eruptive period, *Journal of Geophysical Research-Solid Earth*, **116**, B05203.

Alparone, S., Barberi, G., Bonforte, A., Maiolino, V., & Ursino, A., 2011. Evidence of multiple strain fields beneath the eastern flank of Mt. Etna volcano (Sicily, Italy) deduced from seismic and geodetic data during 2003-2004, *Bulletin of Volcanology*, **73**(7), 869–885.

Argnani, A., Mazzarini, F., Bonazzi, C., Bisson, M., & Isola, I., 2011. The deformation offshore of Mount Etna as imaged by multichannel seismic reflection profiles, submitted to *Journal of Volcanology and Geothermal Research*.

Battaglia, M., Di Bari, M., Acocella, V., & Neri, M., 2011. Dike emplacement and flank instability at Mount Etna: Constraints from a poro-elastic-model of flank collapse, *Journal Of Volcanology And Geothermal Research*, **199**(1-2), 153–164.

Bonaccorso, A., Cianetti, S., Giunchi, C., Trasatti, E., Bonafede, M., & Boschi, E., 2005. Analytical and 3-D numerical modelling of Mt. Etna (Italy) volcano inflation, *Geophysical Journal International*, **163**(2), 852–862.

Bonaccorso, A., Bonforte, A., Currenti, G., Del Negro, C., Di Stefano, A., & Greco, F., 2011. Magma storage, eruptive activity and flank instability: Inferences from ground deformation and gravity changes during the 1993-2000 recharging of Mt. Etna volcano, *Journal Of Volcanology And Geothermal Research*, **200**(3-4), 245–254.

Bonforte, A. & Puglisi, G., 2006. Dynamics of the eastern flank of Mt. Etna volcano (Italy) investigated by a dense GPS network, *Journal Of Volcanology And Geothermal Research*, **153**(3-4), 357–369.

Bonforte, A., Bonaccorso, A., Guglielmino, F., Palano, M., & Puglisi, G., 2008. Feeding system and magma storage beneath Mt. Etna as revealed by recent inflation/deflation cycles, *Journal of Geophysical Research-Solid Earth*, **113**(B5), B05406.

Bonforte, A., Guglielmino, F., Coltelli, M., Ferretti, A., & Puglisi, G., 2011. Structural assessment of Mount Etna volcano from Permanent Scatterers analysis, *Geochemistry Geophysics Geosystems*, **12**, Q02002.

Borgia, A., Ferrari, L., & Pasquarè, G., 1992. Importance of Gravitational Spreading in the Tectonic and Volcanic Evolution of Mount Etna, *Nature*, **357**(6375), 231–235.

Bousquet, J. C. & Lanzafame, G., 2004. The tectonics and geodynamics of Mt. Etna: Synthesis and interpretation of geological and geophysical data, in *Mt. Etna: Volcano Laboratory*, pp. 29–47, AGU, Washington, DC.

Branca, S., Carbone, D., & Greco, F., 2003. Intrusive mechanism of the 2002 NE-Rift eruption at Mt. Etna (Italy) inferred through continuous microgravity data and volcanological evidences, *Geophysical*

Research Letters, **30**(20), 2077.

Chiarabba, C., De Gori, P., & Patanè, D., 2004. The Mt. Etna plumbing system: The contribution of seismic tomography, in *Mt. Etna: Volcano Laboratory*, pp. 191–204, AGU, Washington, DC.

Chiocci, F. L., Coltelli, M., Bosman, A., & Cavallaro, D., 2011. Continental margin large-scale instability controlling the flank sliding of Etna volcano, *Earth and Planetary Science Letters*, **305**(1-2), 57–64.

Cianetti, S., Tinti, E., Giunchi, C., & Cocco, M., 2008. Modelling deformation rates in the western Gulf of Corinth: rheological constraints, *Geophysical Journal International*, **174**(2), 749–757.

Corsaro, R. & Pompilio, M., 2004. Buoyancy-controlled eruption at Mt. Etna, *Terranova*, **16**, 16–22.

Currenti, G., Del Negro, C., & Ganci, G., 2007. Modelling of ground deformation and gravity fields using finite element method: an application to Etna volcano, *Geophysical Journal International*, **169**(2), 775–786.

Currenti, G., Bonaccorso, A., Del Negro, C., Scandura, D., & Boschi, E., 2010. Elasto-plastic modeling of volcano ground deformation, *Earth and Planetary Science Letters*, **296**(3-4), 311–318.

Davis, P., 1986. Surface Deformation Due to Inflation of an Arbitrarily Oriented Triaxial Ellipsoidal Cavity in an Elastic Half-Space, with Reference to Kilauea Volcano, Hawaii, *Journal Of Geophysical Research-Solid Earth And Planets*, **91**, 7429–7438.

De Gori, P., Chiarabba, C., & Patanè, D., 2005. Qp structure of Mount Etna: Constraints for the physics of the plumbing system, *Journal of Geophysical Research-Solid Earth*, **110**(B5), B05303.

Del Negro, C., Currenti, G., & Scandura, D., 2009. Temperature-dependent viscoelastic modeling of ground deformation: Application to Etna volcano during the 1993-1997 inflation period, *Physics Of The Earth And Planetary Interiors*, **172**(3-4), 299–309.

Dieterich, J., 1988. Growth and Persistence of Hawaiian Volcanic Rift Zones, *Journal Of Geophysical Research-Solid Earth And Planets*, **93**, 4258–4270.

Gambino, S., Mostaccio, A., Patanè, D., Scarfì, L., & Ursino, A., 2004. High-precision locations of the microseismicity preceding the 2002-2003 Mt. Etna eruption, *Geophysical Research Letters*, **31**(18), L18604.

Heap, M. J., Baud, P., Meredith, P. G., Vinciguerra, S., Bell, A. F., & Main, I. G., 2011. Brittle creep in basalt and its application to time-dependent volcano deformation, *Earth and Planetary Science Letters*, **307**(1-2), 71–82.

Lundgren, P. & Rosen, P., 2003. Source model for the 2001 flank eruption of Mt. Etna volcano, *Geophysical Research Letters*, **30**(7), 1388.

Lundgren, P., Casu, F., Manzo, M., Pepe, A., Berardino, P., Sansosti, E., & Lanari, R., 2004. Gravity and magma induced spreading of Mount Etna volcano revealed by satellite radar interferometry, *Geophysical Research Letters*, **31**(4), L04602.

McGuire, W., 1996. Volcano instability: a review of contemporary themes, *Geological Society, London,*

Special Publications, **110**(1), 1–23.

Mogi, K., 1958. Relation between the eruptions of various volcanoes and deformations of the ground surfaces around them, *Bull. Earth Res. Inst.*, **36**, 99–134.

Mollo, S., Vinciguerra, S., Iezzi, G., Iarocci, A., Scarlato, P., Heap, M. J., & Dingwell, D. B., 2011. Volcanic edifice weakening via devolatilization reactions, *Geophysical Journal International*, **186**(3), 1073–1077.

Monaco, C., De Guidi, G., & Ferlito, C., 2010. The Morphotectonic map of Mt. Etna, *Italian Journal Of Geosciences*, **129**(3), 408–428.

Neri, M. & Rossi, M., 2002. Geometria e Volume dell'apparato vulcanico etneo: il contributo offerto dall'uso di mappe digitali, *Quaderni di Geofisica*, **20**, 1–16.

Neri, M., Acocella, V., Behncke, B., Maiolino, V., Ursino, A., & Velardita, R., 2005. Contrasting triggering mechanisms of the 2001 and 2002-2003 eruptions of Mount Etna (Italy), *Journal Of Volcanology And Geothermal Research*, **144**(1-4), 235–255.

Norini, G. & Acocella, V., 2011. Analogue modeling of flank instability at Mount Etna: Understanding the driving factors, *Journal of Geophysical Research-Solid Earth*, **116**, B07206.

Palano, M., Puglisi, G., & Gresta, S., 2008. Ground deformation patterns at Mt. Etna from 1993 to 2000 from joint use of InSAR and GPS techniques, *Journal Of Volcanology And Geothermal Research*, **169**(3-4), 99–120.

Palano, M., Rossi, M., Cannavò, F., Bruno, V., Aloisi, M., Pellegrino, D., Pulvirenti, M., Siligato, G., & Mattia, M., 2010. Etn@ref: a geodetic reference frame for Mt. Etna GPS networks, *Annals Of Geophysics*, **53**(4), 49–57.

Pareschi, M. T., Boschi, E., Mazzarini, F., & Favalli, M., 2006. Large submarine landslides offshore Mt. Etna, *Geophysical Research Letters*, **33**(13), L13302.

Patanè, D., De Gori, P., Chiarabba, C., & Bonaccorso, A., 2003. Magma ascent and the pressurization of Mount Etna's volcanic system, *Science*, **299**(5615), 2061–2063.

Patanè, D., Mattia, M., & Aloisi, M., 2005. Shallow intrusive processes during 2002-2004 and current volcanic activity on Mt. Etna, *Geophysical Research Letters*, **32**(6), L06302.

Patanè, D., Barberi, G., Cocina, O., De Gori, P., & Chiarabba, C., 2006. Time-resolved seismic tomography detects magma intrusions at Mount Etna, *Science*, **313**(5788), 821–823.

Peng, S. & Zhang, J., 2007. In-situ stress and pore pressure, in *Engineering Geology for Underground rocks*, pp. 45–74, Springer Berlin Heidelberg.

Puglisi, G., Bonforte, A., Ferretti, A., Guglielmino, F., Palano, M., & Prati, C., 2008. Dynamics of Mount Etna before, during, and after the July-August 2001 eruption inferred from GPS and differential synthetic aperture radar interferometry data, *Journal of Geophysical Research-Solid Earth*, **113**(B6), B06405.

Ruch, J., Acocella, V., Storti, F., Neri, M., Pepe, S., Solaro, G., & Sansosti, E., 2010. Detachment depth

revealed by rollover deformation: An integrated approach at Mount Etna, *Geophysical Research Letters*, **37**, L16304.

Siniscalchi, A., Tripaldi, S., Neri, M., Giammanco, S., Piscitelli, S., Balasco, M., Behncke, B., Magri, C., Naudet, V., & Rizzo, E., 2010. Insights into fluid circulation across the Pernicana Fault (Mt. Etna, Italy) and implications for flank instability, *Journal Of Volcanology And Geothermal Research*, **193**(1-2), 137–142.

Solaro, G., Acocella, V., Pepe, S., Ruch, J., Neri, M., & Sansosti, E., 2010. Anatomy of an unstable volcano from InSAR: Multiple processes affecting flank instability at Mt. Etna, 1994-2008, *Journal of Geophysical Research-Solid Earth*, **115**, B10405.

Tarquini, S., Isola, I., Favalli, M., Mazzarini, F., Bisson, M., Pareschi, M. T., & Boschi, E., 2007. TINITALY/01: a new Triangular Irregular Network of Italy, *Annals Of Geophysics*, **50**(3), 407–425.

Tibaldi, A. & Groppelli, G., 2002. Volcano-tectonic activity along structures of the unstable NE flank of Mt. Etna (Italy) and their possible origin, *Journal Of Volcanology And Geothermal Research*, **115**(3-4), 277–302.

Trasatti, E., Giunchi, C., & Piana Agostinetti, N., 2008. Numerical inversion of deformation caused by pressure sources: application to Mount Etna (Italy), *Geophysical Journal International*, **172**(2), 873–884.

Trasatti, E., Cianetti, S., Giunchi, C., Bonafede, M., Piana Agostinetti, N., Casu, F., & Manzo, M., 2009. Bayesian source inference of the 1993-1997 deformation at Mount Etna (Italy) by numerical solutions, *Geophysical Journal International*, **177**(2), 806–814.

Table 1. Material parameters inferred from measurements of Mount Etna rock samples by S. Vinciguerra at INGV HTPT Lab (*http://www.roma1.ingv.it/laboratories/hp-ht-lab*), see text for details (E, Young modulus; ν, Poisson's ratio; ρ, density; C, cohesion; ϕ, internal friction angle).

Lithotype	E (GPa)	ν	ρ (kg / m^{-3})	C (MPa)	ϕ
Volcanites	30	0.20	2300	43.40	38°
Clay	6	0.27	2500	0.87	30°
Flysch (Sandstones)	16.5	0.30	2500	2.9	30°
Carbonates	35	0.25	2700		
DC	50	0.25	3000		

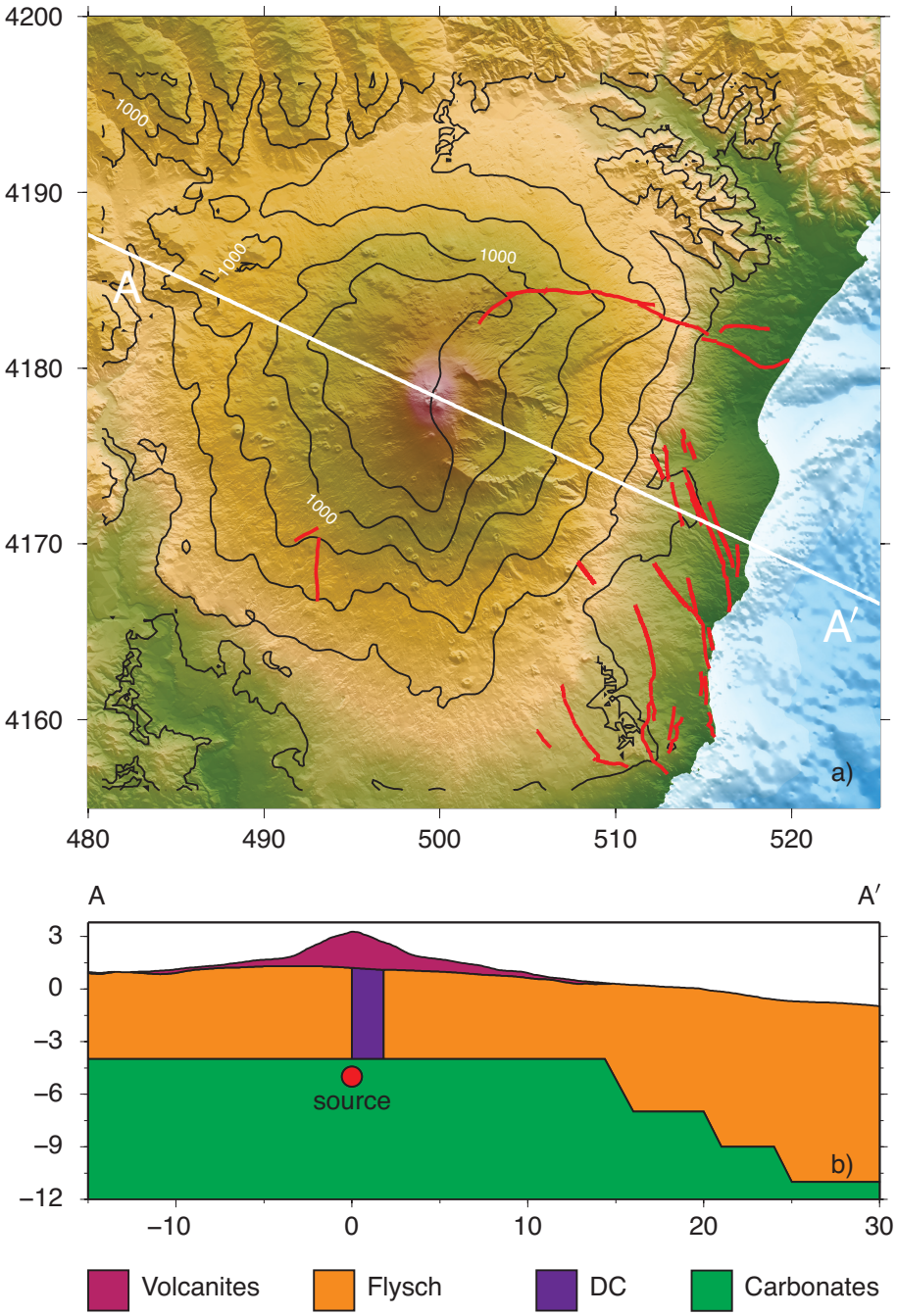

Figure 1. a) Mount Etna topographic relief (Tarquini et al. 2007) and bathymetry (GEBCO, *http://www.gebco.net*) of the Ionian Sea. Solid black lines are contour lines of the top of the sedimentary layer from (Neri & Rossi 2002). Solid red lines are the surface traces of the seismogenic faults by Branca et al. (2003), retrieved in the framework of the FLANK project. The solid line labelled AA′ shows the trace of the 2D cross section in panel b). The reconstruction of internal layering of Mount Etna is explained in the text. The red dot shows the location and dimension of the isotropic source.

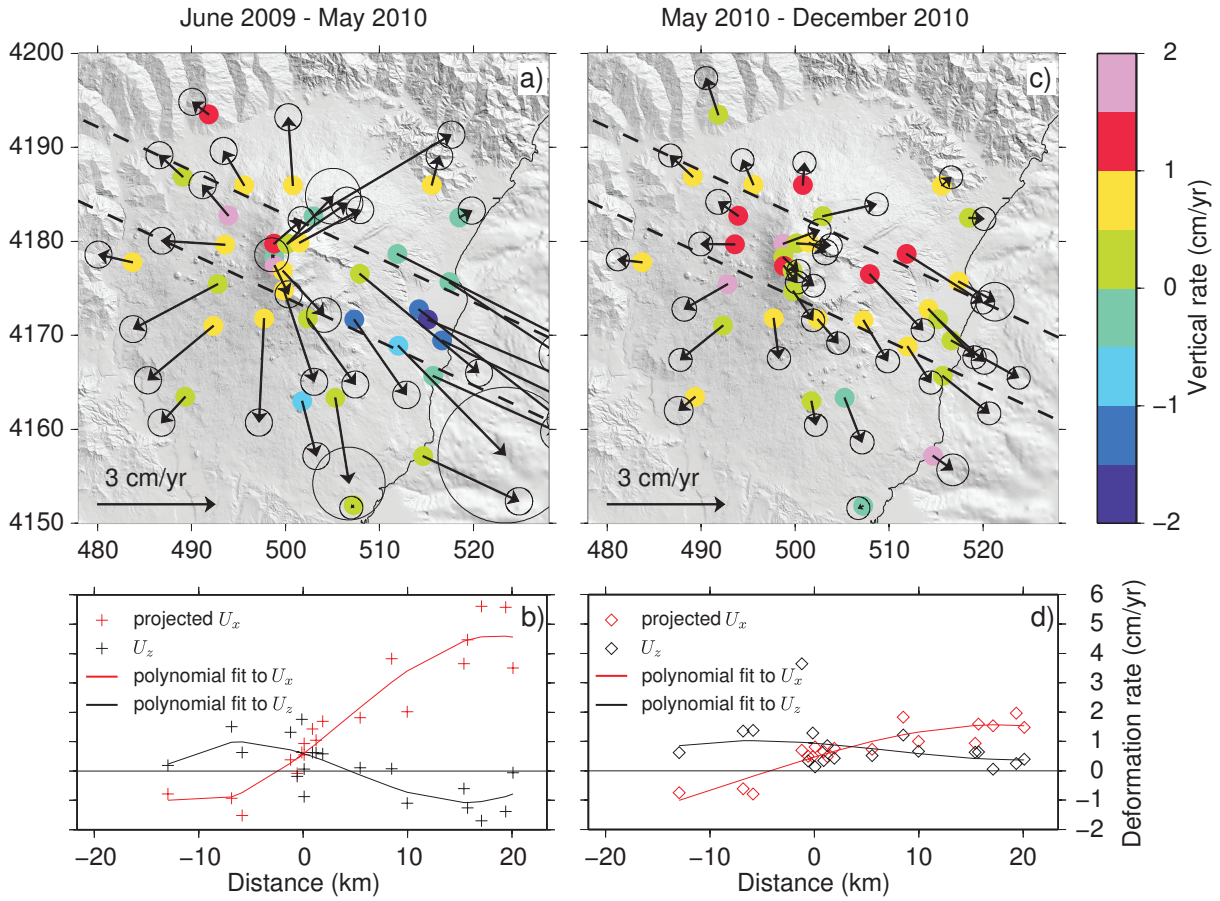

Figure 2. Panels a) and c) show the horizontal (black arrows) and vertical (color circles) deformation rates redrawn from Aloisi et al. (2011b) for the time intervals June 2009–May 2010 and May 2010–December 2010, respectively. The black dashed lines delimit the GPS sites whose distance from the cross-section AA′ (shown in Fig. 1) is less than 4 km. For these benchmarks we compute the horizontal deformation rates along the cross-section AA′ (115° Azimuth). The results are plotted in panels b) and d) as red crosses and diamonds, respectively. Black crosses and diamonds are the corresponding vertical deformation rates. The thin red and black lines represent a cubic polynomial fit to projected U_x and U_z, respectively.

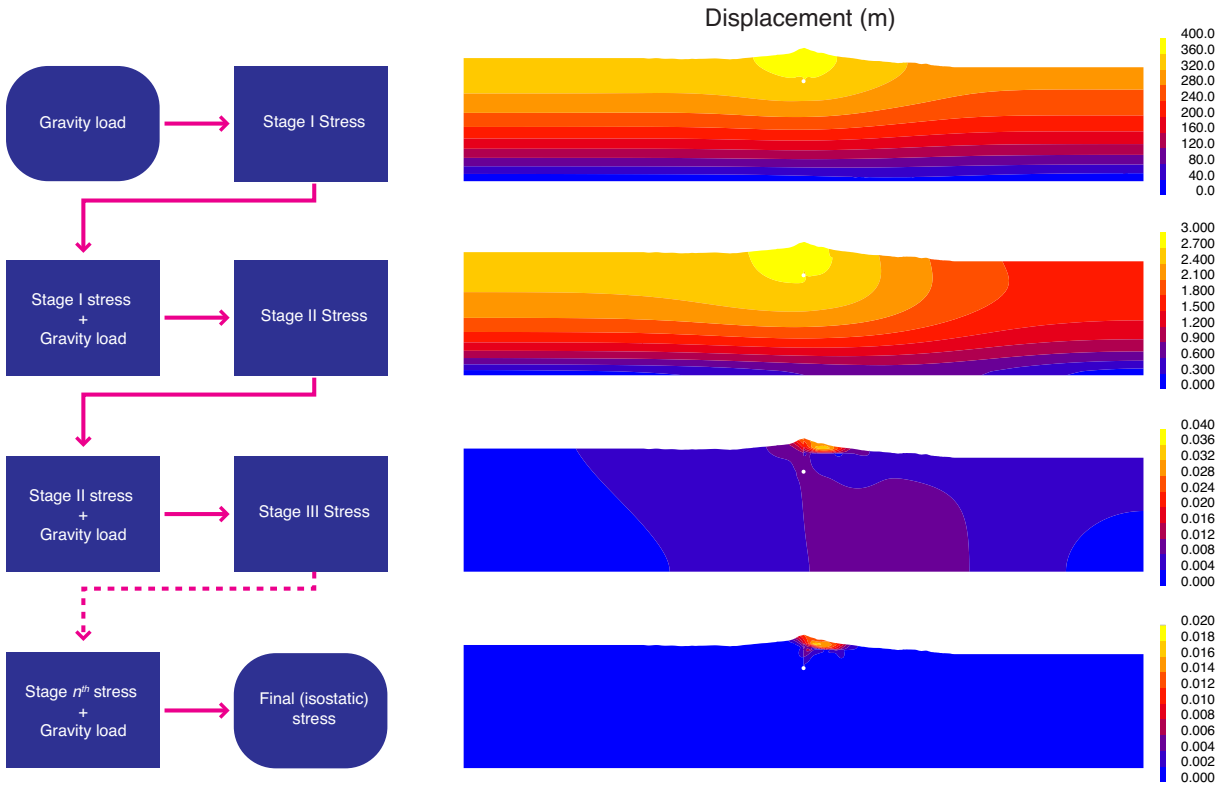

Figure 3. Flow chart describing the iterative procedure to compute the initial state of stress consistent with rheology and heterogeneities assumptions of the models. After each iteration the computed displacement is reduced with respect to the previous step. The final stress field is assumed to be the initial reference stress if the corresponding displacements reach values very small when compared to expected deformation due to active sources. In this specific model of Mount Etna, final displacements are sub-millimetric.

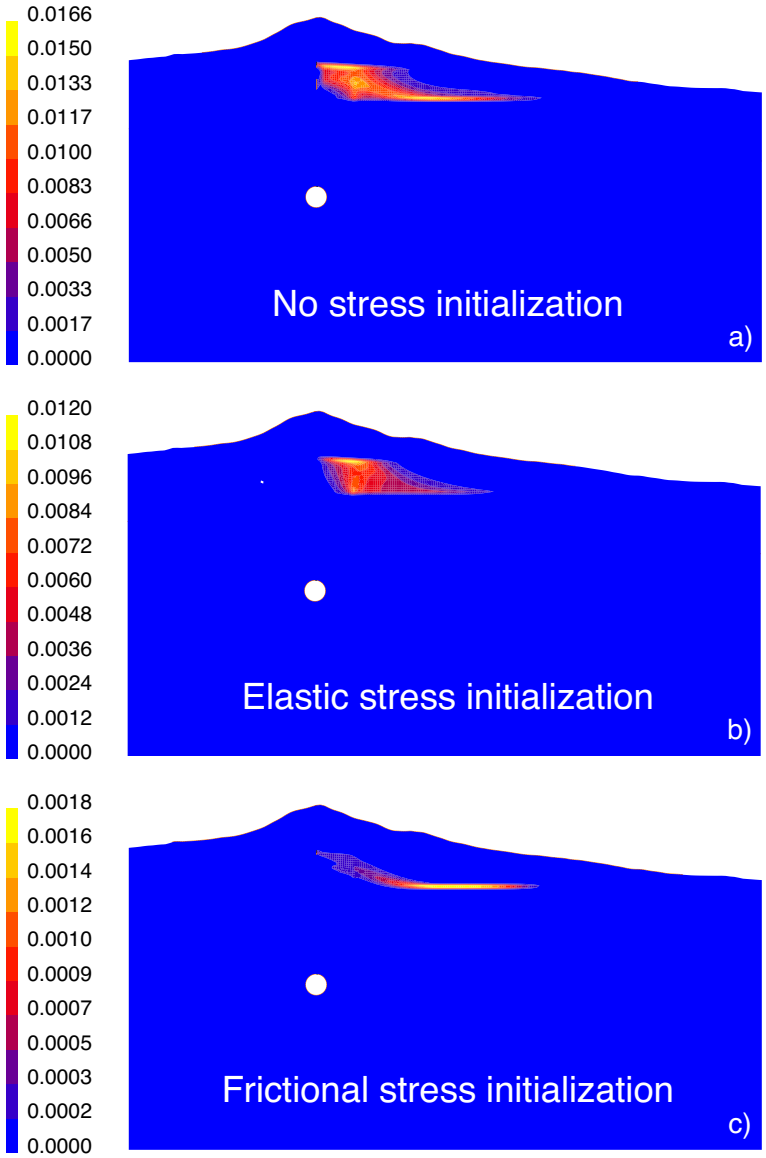

Figure 4. Total equivalent plastic strain resulting from different hypothesis about initial stress. See Sec. 3.4 for details.

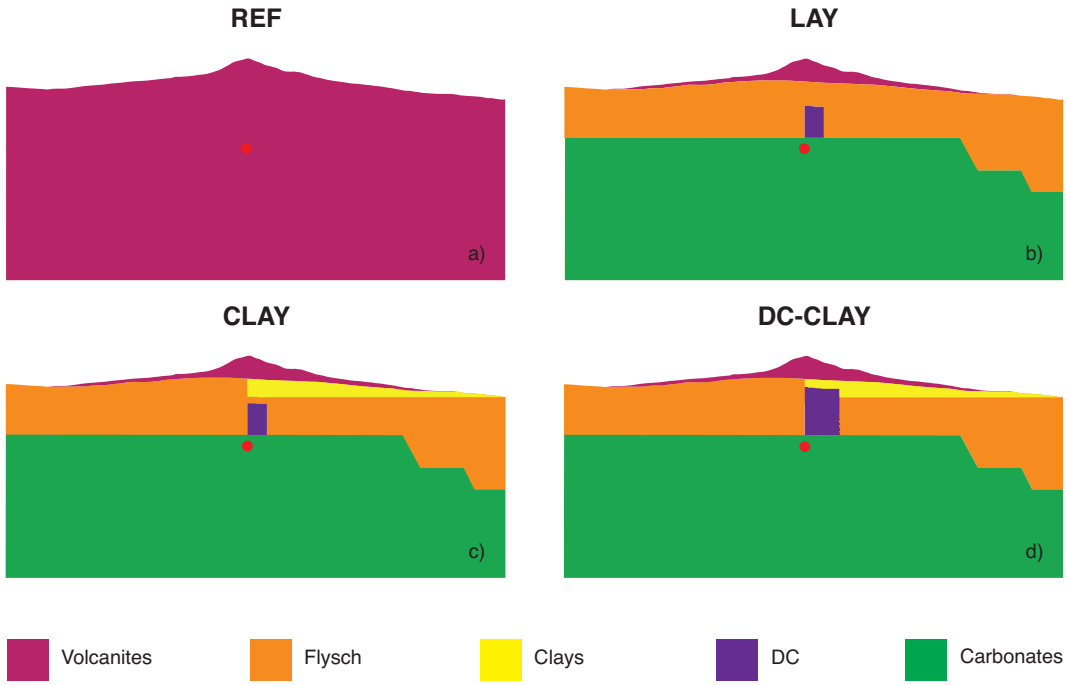

Figure 5. Sketches of the investigated models including lithotypes and geometry of layers. All the models include both topography (Tarquini et al. 2007) and the GEBCO bathymetry (*http://www.gebco.net*): a) REF uniform, homogeneous model ; b) LAY, includes the major lithotypes characterizing the internal structure of Mount Etna together with a dike complex (DC) body located east of the central craters; c) CLAY, identical to LAY but with the presence of the unconsolidated clay layer; d) DC-CLAY, identical to CLAY but with increased DC dimensions.

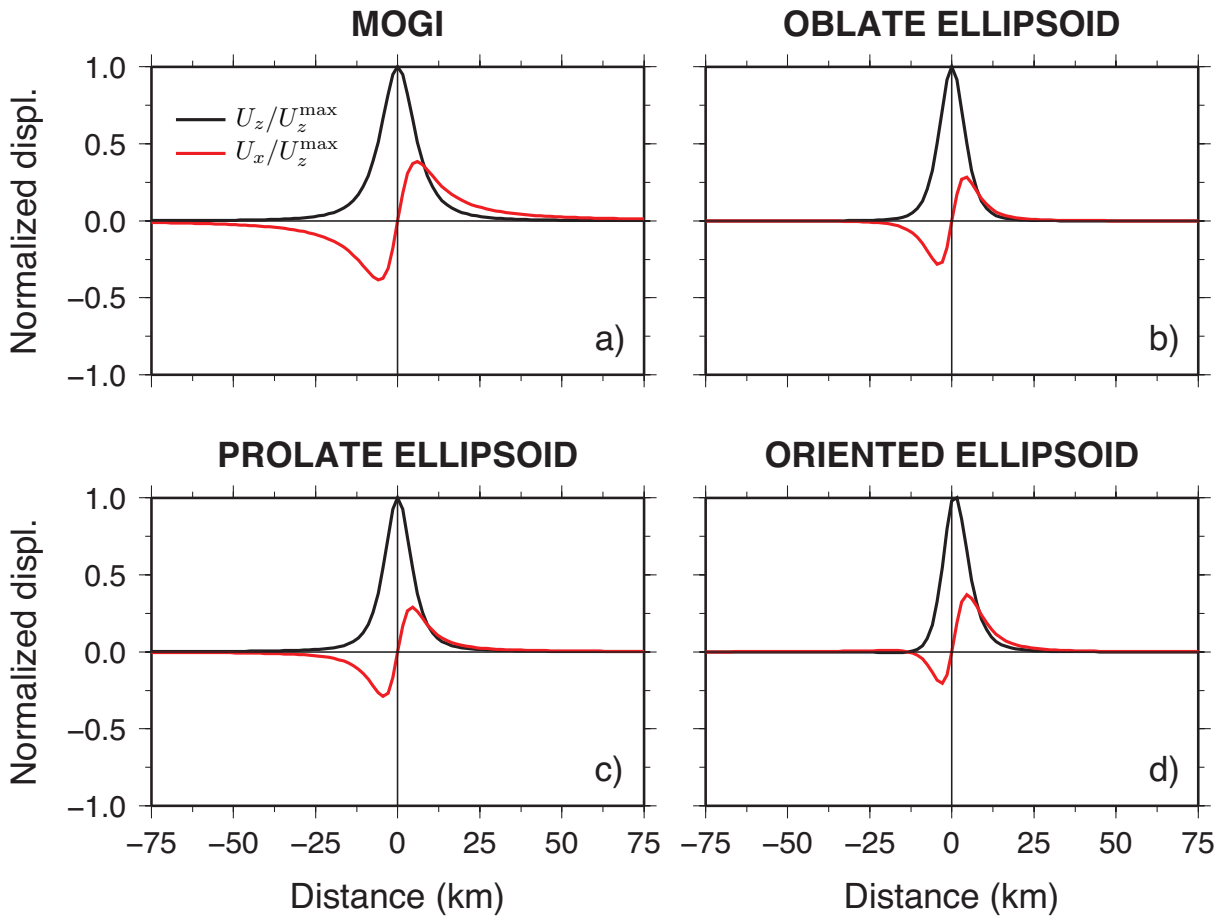

Figure 6. Normalized horizontal (solid red lines) and vertical (solid black lines) displacements for analytical models of magmatic sources (Mogi 1958; Davis 1986) along the AA′ section of Fig. 1.

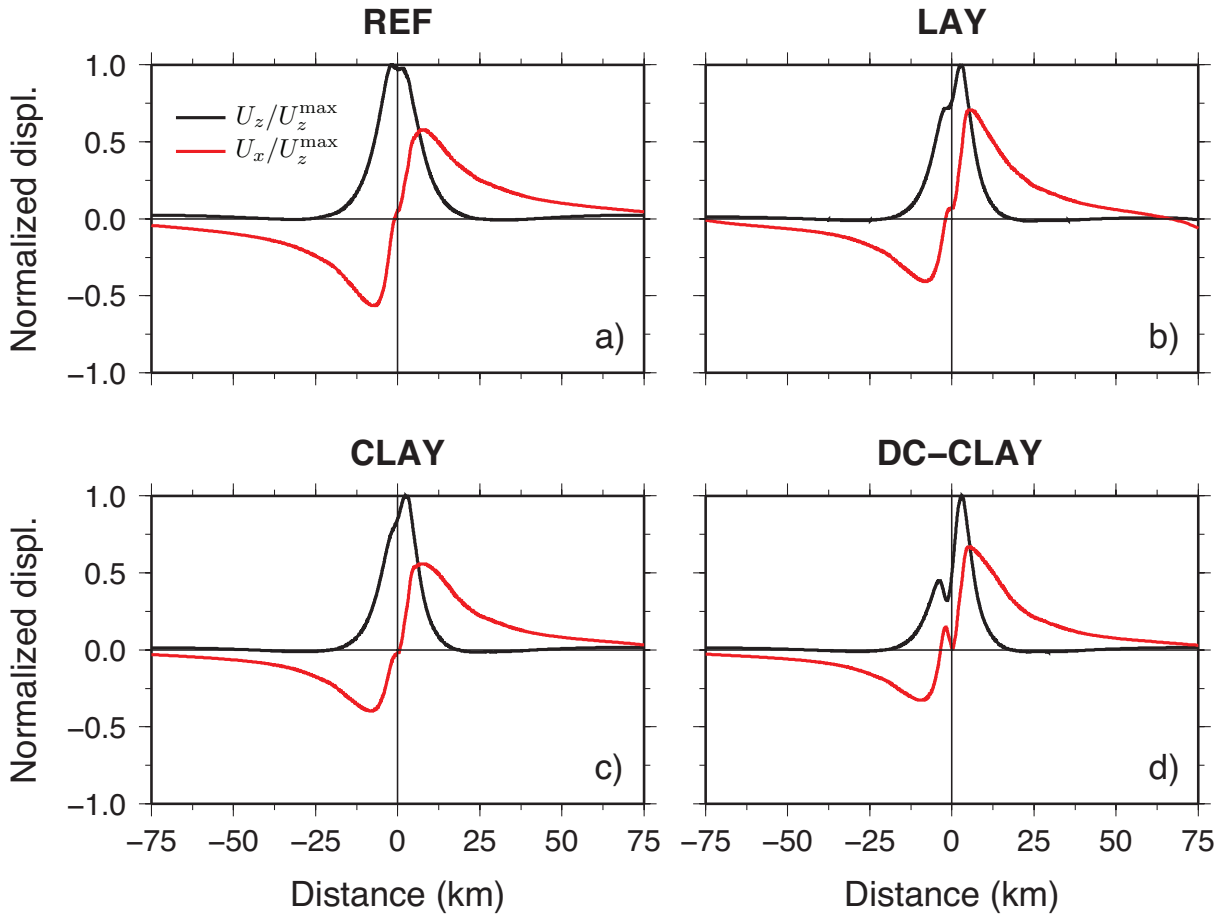

Figure 7. Normalized horizontal (solid red lines) and vertical (solid black lines) displacements predicted by the models described in Fig. 5. The deformation is induced by a spherical, isotropic source common to all models.

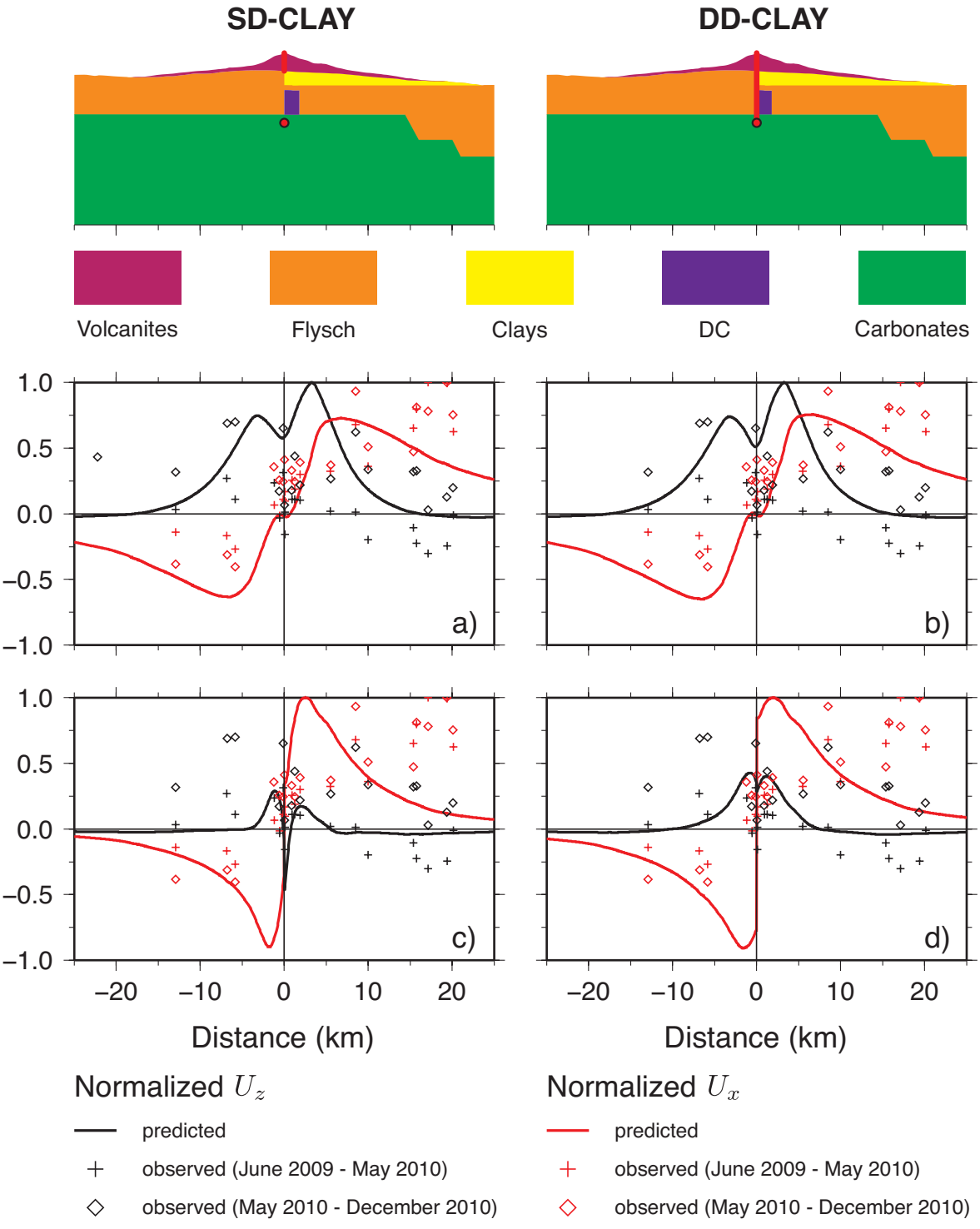

Figure 8. Normalized horizontal (red thick lines) and vertical (black thick lines) displacements predicted by the models with shallow dike (SD-CLAY) and deep dike (DD-CLAY) for a pressurized source [a), b)] and dike opening [c), d)]. Crosses and diamonds are the projections of the normalized displacements from Aloisi et al. (2011b) for the two episodes June 2009-May 2010 and May 2010-December 2010, respectively. Red and black colors are for horizontal and vertical components, respectively. The GPS sites are those confined within the black dashed lines in Fig. 2a. The normalization factor is either the maximum vertical displacement $U_z^{\max}$ [a), b)] or maximum horizontal displacement $U_x^{\max}$ [c), d)], according to the two types of active sources.

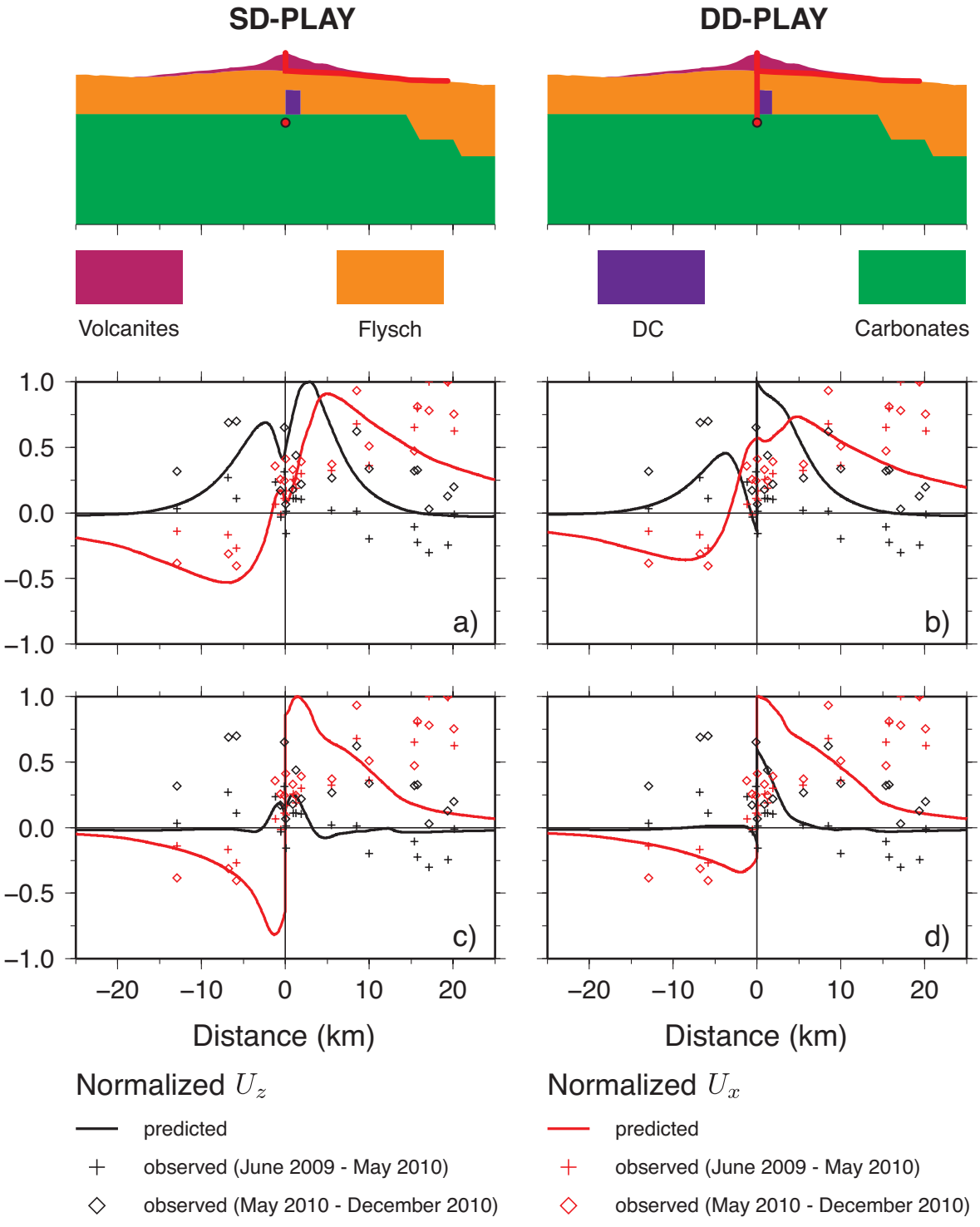

Figure 9. The same as in Fig. 8 for SD-PLAY and DD-PLAY models.

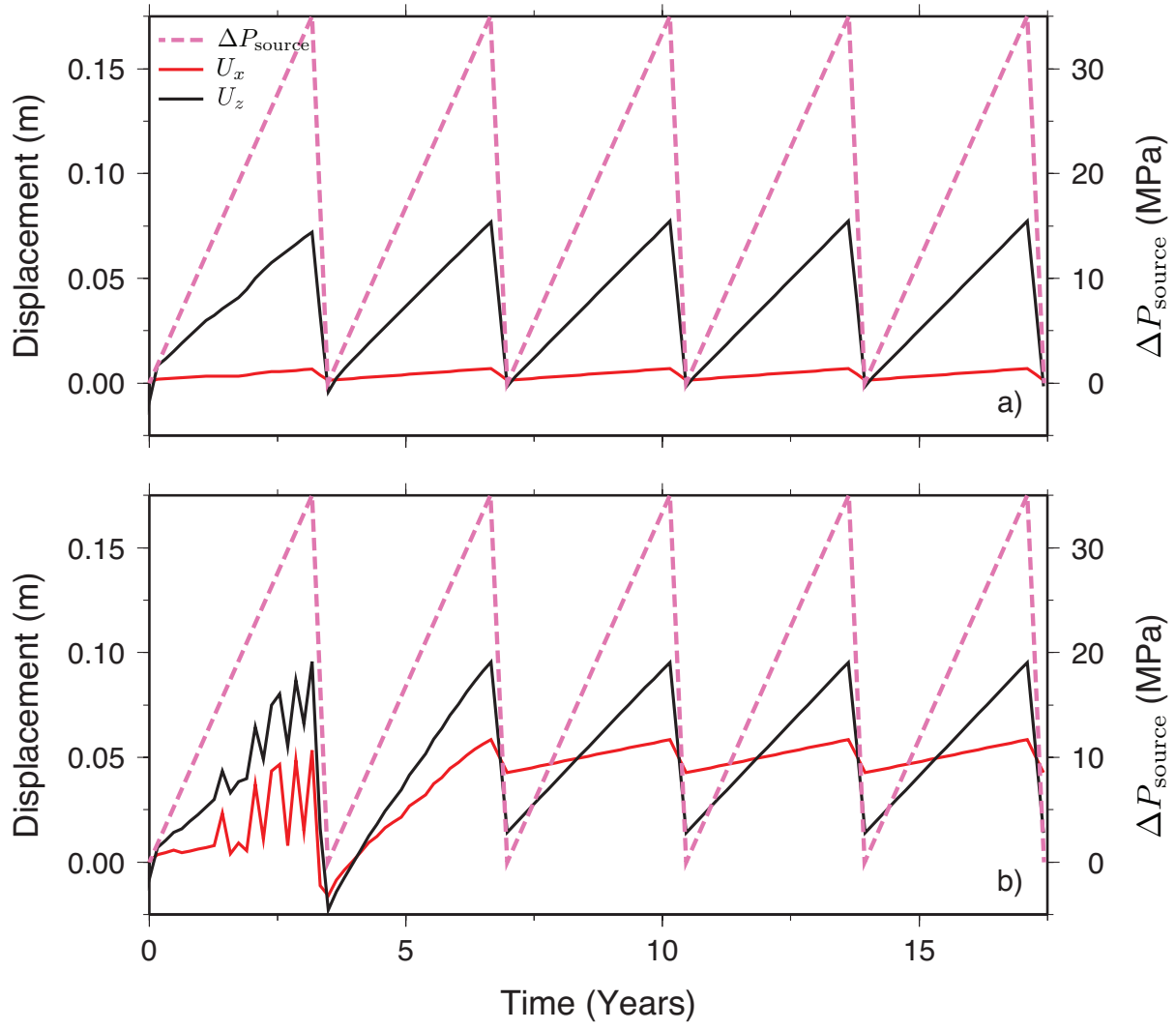

Figure 10. Displacement history of a node located on the surface, 1.4 km east of the source center, compared to applied pressure at magmatic source. We assume that the volcano experiences repeated inflation/deflation cycles. Top: model DD-CLAY; Bottom: model DD-PLAY. Solid red line is for U_x (m) solid black for U_z (m) and purple dashed is for ΔP_{source} (MPa).